

Massive Multi-species, Multi-level NLTE Model Atmospheres for Novae in Outburst

C. Ian Short and Peter H. Hauschildt

Dept. of Physics and Astronomy and Center for Simulational Physics, University of
Georgia, Athens, GA 30602-2451

and

E. Baron

Dept. of Physics and Astronomy, University of Oklahoma, 440 W. Brooks, Rm 131,
Norman, OK 73091-0225

ABSTRACT

We have used our PHOENIX multi-purpose model atmosphere code to calculate atmospheric models that represent novae in the optically thick wind phases of their outburst. We have improved the treatment of NLTE effects by expanding the number of elements that are included in the calculations from 15 to 19, and the number of ionization stages from 36 to 87. The code can now treat a total of 10713 levels and 102646 lines in NLTE. Aluminum, P, K, and Ni are included for the first time in the NLTE treatment and most elements now have at least the lowest six ionization stages included in the NLTE calculation. We have investigated the effects of expanded NLTE treatment on the chemical concentration of astrophysically significant species in the atmosphere, the equilibrium structure of the atmosphere, and the emergent flux distribution. Although we have found general qualitative agreement with previous, more limited NLTE models, the expanded NLTE treatment leads to significantly different values for the size of many of the NLTE deviations. In particular, for the hottest model presented here ($T_{\text{eff}} = 35\,000$ K), for which NLTE effects are largest, we find that the expanded NLTE treatment *reduces* the NLTE effects for these important variables: H I concentration, pressure structure, and emergent far *UV* flux. Moreover, we find that the addition of new NLTE species may greatly affect the concentration of species that were already treated in NLTE, so that, generally, *all* species that contribute significantly to the e^- reservoir or to the total opacity, or whose line spectrum overlaps or interlocks with that of a species of interest, must be treated in NLTE to insure an accurate result for any particular species.

Subject headings: novae, cataclysmic variables — radiative transfer — stars:
atmospheres

1. Introduction

Novae in the optically thick wind phase of their outburst pose a special challenge for atmospheric modeling because of their steep temperature gradients, low densities, large geometric extents, and high velocity differential flows. For example, a model with a bolometrically defined effective temperature, T_{eff} , of 15 000 K will have values of the kinetic temperature, T_{kin} , that range from 4500 to 140 000 K, of the mass density, ρ , that range from 3×10^{-15} to 6×10^{-9} g cm $^{-3}$, a geometric extent, $R_{\text{out}}/R_{\text{in}}$, equal to 120 (this paper), and a typical maximum expansion velocity, V_0 , of ≈ 2000 km s $^{-1}$. Because of the low values of ρ , radiative rates exceed collisional rates for many important transitions throughout the atmosphere. The steep T_{kin} gradient and low densities allow local regions to be exposed through scattering processes to radiation from distant regions in the atmosphere where the radiation temperature, T_{rad} , differs greatly from the local value of T_{kin} . Moreover, massive ultraviolet (UV) and optical line blanketing cause the radiation field to deviate greatly from a Planck (B_ν) distribution. As a result of these considerations, non-local thermodynamic equilibrium (NLTE) effects are severe in these atmospheres and must be accounted for to construct accurate models. The low values of ρ cause the atmosphere to be translucent ($\tau < 1$) at large physical depths, which, combined with the large absolute value of $\nabla_\tau T$, conspires to allow the line spectrum of many ionization stages of an atomic element to be present in the emergent flux spectrum. Moreover, the rapid expansion velocities and steep $v(r)$ gradients cause this rich line spectrum to be smeared, which complicates the radiative transfer by increasing the amount of overlap among different transitions. Also, the large velocities cause special relativistic effects to be marginally significant in the transfer of radiation, at least to first order in v/c . Finally, the large geometric extent allows sphericity effects to be important.

Hauschildt *et al.* 1995, and Hauschildt *et al.* 1997b, (henceforth HSSBSA) investigated the effects of NLTE on atmospheric models of novae in the optically thick wind phase of their outburst. They concluded that an accurate treatment of NLTE effects for many transitions is critical for correctly calculating both the structure of the atmosphere and the emergent flux spectrum. Among their main results are that: 1) NLTE effects change the predicted concentration of minority ionization stages of elements that contribute significantly to the

line opacity, such as Fe and CNO, by as much as three orders of magnitude at depths where the continuum optical depth at 5000\AA , $\tau_{\text{cont},5000}$, is less than 10^{-2} , 2) NLTE effects brighten the predicted *UV* pseudo-continuum by as much as an order of magnitude in the case of their 25 000 K model in the range $\lambda < 1000\text{\AA}$, and 3) a minimal incorporation of NLTE physics by including a large single scattering albedo in the line source functions of an LTE synthetic spectrum gives rise to a spectrum with approximately the same overall level of line blanketing absorption as a more complete NLTE treatment, although any individual line profile may be inaccurate. HSSBSA concluded that their NLTE models provided a better fit to observed spectra of novae.

One of the limitations of the modeling of Hauschildt *et al.* 1995 and HSSBSA is the limited number of elements and ionization stages treated in NLTE (15 elements and 36 stages). Given the importance of NLTE effects, we have increased the NLTE treatment to include 19 elements and 87 ionization stages. In Section 2 we describe the NLTE treatment, in Section 3 we describe the nova models, in Section 4 we present the results of our calculations, and in Section 5 we present our conclusions.

2. NLTE Treatment

Table 1 shows the *complete* set of chemical elements and ionization stages now treated in NLTE by PHOENIX along with the number of levels and primary bound-bound transitions included in the model atoms and ions. Primary transitions are those that connect states with observed energy levels and that have a $\log gf$ value greater than -3.0 . They are explicitly treated in the NLTE rate equations. All other transitions of a species treated in NLTE are considered secondary. Secondary transitions are not included in the rate equations, but are still included in the line opacity, with the departure co-efficients of any levels not included in the rate equations set equal to that of the ground state (see Hauschildt and Baron 1995 for a detailed description). New species are denoted in bold face type and species for which the treatment has been improved with enlarged model atoms are denoted with italics. We have added four new elements and 51 new ionization stages to the NLTE treatment with the result that the code can now treat a total of 87 ionization stages among 19 elements. This has increased the number of levels and lines included in the statistical equilibrium solution by 5415 and 42521, respectively, thereby approximately doubling the total numbers included. Aluminum, P, K, and Ni are now included in the NLTE treatment for the first time. The latter is important for supernova modeling because of the role of the radio-active decay of Ni in the energy balance of SNe

Table 1. Species and number of levels and primary transitions treated in NLTE.

Element	Ionization Stage						
	I	II	III	IV	V	VI	VII
<i>H</i>	<i>80/3160^a</i>
He	19/37	10/45
Li	57/333	55/124
C	228/1387	85/336	79/365	35/171
N	252/2313	152/1110	87/266	80/388	39/206	15/23	...
O	36/66	171/1304	137/765	134/415	97/452	39/196	...
Ne	26/37
<i>Na</i>	<i>53/142</i>	35/171	69/353	46/110	64/187	102/375	...
<i>Mg</i>	273/835	<i>72/340</i>	91/656	54/169	53/133	78/180	...
Al	111/250	188/1674	58/297	31/142	49/77	40/93	...
Si	329/1871	93/436	155/1027	52/292	35/125	36/49	...
P	229/903	89/760	51/145	50/174	40/204	10/9	...
S	146/439	84/444	41/170	28/50	19/41	31/144	...
K	73/210	22/66	38/178	24/57	29/75
Ca	194/1029	87/455	150/1661	67/122	39/91	23/37	26/59
Ti	395/5279	204/2399
Fe	494/6903	617/13675	566/9721	243/2592	132/961	87/551	...
Co	316/4428	255/2725	213/2248
Ni	153/1690	429/7445	259/3672	189/1845	245/2638	246/2868	...
Total	10713/102646						

Note. — New elements and stages are indicated with bold face text. Species for which the model atom or ion has been improved are denoted with italics.

^aOnly 30 levels used in model (see text).

envelopes, but is inconsequential for the nova modeling described here. Most elements now have at least the lowest six ionization stages treated in NLTE. For most elements this level of ionization corresponds to an energy in the range of 100 to 200 eV, which is well above the local thermal energy in the atmospheres of the hottest novae that we have modeled. In addition, we have improved the NLTE treatment of Na I and Mg II by enlarging the model atoms from three levels and two lines to 53 levels and 142 lines for Na I, and from 18 levels and 37 lines to 273 levels and 835 lines for Mg II.

We have also enlarged the H I model atom from 30 levels and 435 lines to 80 levels and 3160 lines. However, we restrict the models to 30 levels of H I because our treatment of dissolution effects among high lying levels is only approximate. These dissolution effects have been shown by Hubeny *et al.* 1994 to have an important effect on model structure and synthetic spectra for models of main sequence stars in the temperature range being investigated here. We note that because Novae atmospheres are expanding rapidly, the gas pressure in the line forming region is orders of magnitude less than that of a static White Dwarf (WD) star. Therefore, we expect dissolution effects to be negligible for states with principal quantum number, n , less than 30.

Atomic data for the energy levels and $b - b$ transitions have been taken from Kurucz (Kurucz 1994, Kurucz and Bell 1995). An accurate treatment of photo-ionization is important for the correct solution of the opacity and chemical equilibrium of a NLTE gas. We have used the resonance averaged Opacity Project (Seaton *et al.* 1994) data of Bautista *et al.* (1998) for the ground state photo-ionization cross sections for Li I- II, C I- IV, N I- VI, O I- VI, Ne I, Na I- VI, I- VI, Al I- VI, Si I- VI, S I- VI, Ca I- VII, and Fe I- VI. These data also incorporate X -ray band opacity due to ionizations from the K electron shell. For those species that were already included in the PHOENIX NLTE treatment, the use of this $b - f$ opacity data is an improvement. For the ground states of all stages of P, Ti, Co, and Ni, and for the *excited* states of *all* species, we have used the cross sectional data previously incorporated into PHOENIX, which are those of Reilman & Manson (Reilman and Manson 1979) or those compiled by Mathisen (Mathisen 1984). We account for coupling among all bound levels by electronic collisions using cross-sections calculated with the formula of Allen (1973), except for those levels connected by radiative transitions, for which we use the formula of Van Regemorter (1962). The cross sections of ionizing collisions with electrons are calculated with the formula of Drawin (1961).

With the expanded NLTE treatment, PHOENIX now treats simultaneously ~ 10000 levels and $\sim 100\,000$ primary transitions in NLTE. This massive NLTE treatment is made possible by the efficiency of the operator splitting method for solving the multi-level NLTE rate equations (Hauschildt 1993) and of the ALI/OS method for solving the radiative transfer equation (Hauschildt 1992), and by the parallel implementation of PHOENIX (Hauschildt *et al.* 1997a, Baron and Hauschildt 1998).

3. Models

We have calculated three models, designated *M1*, *M2*, and *M3*, that represent the state of a nova at three different times during the optically thick wind phase of the outburst. Table 2 presents some of the model parameters. During the optically thick wind phase, the radius at which $\tau_{\text{cont},5000}$ equals unity is decreasing due to the decrease in ρ as the atmosphere expands. The decreasing value of ρ also allows energetic photons from the central engine to penetrate further out into the expanding atmosphere, thereby increasing T_{eff} . For these spherically extended atmospheres the value of T_{eff} is defined as the model temperature that corresponds to the total frequency integrated luminosity ($\sigma T_{\text{eff}}^4 = \frac{3}{4\pi R_{\tau=1}^2} \int_0^\infty L_\nu d\nu$). During this phase, the photospheric radius, $r(\tau_{\text{cont},5000} = 1)$, and T_{eff} change such that the bolometric luminosity, L_{bol} , remains constant. For our models, L_{bol} is equal to $50\,000 L_\odot$. The optical depth grid contains 50 points and spans the range from a $\log \tau_{\text{cont},5000}$ value of -10 to three. Because of the decline in ρ , a fixed grid in τ space corresponds to a contracting grid in physical distance space. However, note that the inner radius at the bottom of the model, R_{in} , decreases faster than the outer radius at the top of the model, R_{out} , so that the geometric extent $R_{\text{out}}/R_{\text{in}}$, and, therefore, the sphericity, of the model is increasing with time. The density law, $\rho(r) = \rho_0(r/R_0)^{-n}$, is prescribed and has a value of $n = 3$. The velocity law, $v(r) = v_0(r/R_0)$, corresponds to a constant mass loss rate ($\dot{M}(r) = \text{constant}$), and has a value of v_0 equal to 2000 km s^{-1} .

For each of these models we have calculated a converged solution for the atmospheric structure that is subject to the constraint of radiative equilibrium for three cases: 1)

Table 2: Parameters of the nova atmospheres

Model	Time	T_{eff} (K)	$r(\tau_{\text{cont},5000} = 1)$ (cm)	L_{bol} (L_\odot)	$R_{\text{out}}/R_{\text{in}}$	v_0 (km s^{-1})
<i>M1</i>	t_1	15 000	2.3×10^{12}	50 000	120	2000
<i>M2</i>	t_2	25 000	8.3×10^{11}	50 000	210	2000
<i>M3</i>	t_3	35 000	4.2×10^{11}	50 000	270	2000

Table 3. Species treated in NLTE for each model in the HSSBSA and current calculations

Element	Ionization Stage						
	I	II	III	IV	V	VI	VII
<i>H</i>	HS/ <i>M1/M2/M3</i>
He	HS/ <i>M1/M2/M3</i>	HS/ <i>M1/M2/M3</i>
Li	None	None
C	HS/ <i>M1/M2/M3</i>	HS/ <i>M1/M2/M3</i>	HS/ <i>M1/M2/M3</i>	HS/ <i>M1/M2/M3</i>
N	<i>M1/M2/M3</i>	<i>M1/M2/M3</i>	<i>M1/M2/M3</i>	<i>M1/M2/M3</i>	<i>M3</i>	None	...
O	<i>M1/M2/M3</i>	<i>M1/M2/M3</i>	<i>M1/M2/M3</i>	<i>M1/M2/M3</i>	<i>M3</i>	None	...
Ne	<i>M1/M2/M3</i>
<i>Na</i>	<i>M1/M2/M3</i>	<i>M1/M2/M3</i>	<i>M1/M2/M3</i>	<i>M1/M2/M3</i>	None	None	...
<i>Mg</i>	<i>M1/M2</i>	HS/ <i>M1/M2/M3</i>	<i>M1/M2/M3</i>	<i>M1/M2/M3</i>	None	None	...
Al	<i>M1/M2/M3</i>	<i>M1/M2/M3</i>	<i>M1/M2/M3</i>	<i>M1/M2/M3</i>	None	None	...
Si	<i>M1/M2</i>	<i>M1/M2/M3</i>	<i>M1/M2/M3</i>	<i>M1/M2/M3</i>	<i>M3</i>	None	...
P	<i>M1/M2</i>	<i>M1/M2/M3</i>	<i>M1/M2/M3</i>	<i>M1/M2/M3</i>	<i>M3</i>	None	...
S	<i>M1/M2</i>	<i>M1/M2/M3</i>	<i>M1/M2/M3</i>	<i>M1/M2/M3</i>	<i>M3</i>	None	...
K	None	None	None	None	None
Ca	<i>M1/M2</i>	HS/ <i>M1/M2/M3</i>	<i>M1/M2/M3</i>	<i>M1/M2/M3</i>	<i>M3</i>	None	None
Ti	None	None
Fe	<i>M1/M2</i>	HS/ <i>M1/M2/M3</i>	<i>M1/M2/M3</i>	<i>M1/M2/M3</i>	<i>M3</i>	None	...
Co	None	None	None
Ni	None	None	None	None	None	None	...

Note. — HS denotes the modeling of HSSBSA. *M1*, *M2*, and *M3* are defined in Table 2.

quasi-LTE treatment for all species in which the Boltzmann and Saha distributions are used for the level populations, and all lines are assumed to have an albedo for single scattering of 0.95, 2) NLTE treatment for only the HSSBSA species, which are denoted by normal typeface in Table 1, and 3) NLTE treatment of all relevant species presented in Table 1. The line albedo used for case 1 was found by HSSBSA to be necessary to produce synthetic LTE spectra for nova models in which the line strengths were approximately realistic. For case 3, relevant species are those whose levels have a numerically significant population anywhere in the atmosphere and whose line spectrum is already known to be an important opacity source for determining the atmospheric structure or the appearance of the emergent spectrum. This limit was placed on the number of species treated in NLTE for the sake of computational expediency. Table 3 lists those species treated in NLTE in each case for each model. *Note that for no model are **all** the species in Table 1 treated in NLTE.* In this regard we note that some of the species in Table 1 are not important for Nova modeling, and the facility to treat them in NLTE was added to PHOENIX for the sake of other applications. For cases 2 and 3, the NLTE problem is converged self-consistently with the atmospheric structure.

4. Results

4.1. NLTE populations

Figs. 1 to 4 show a comparison of the partial pressures of various species computed in LTE and with both NLTE treatments for all model. The current NLTE treatment includes all those species indicated in Table 3. Note that changes to the NLTE treatment may affect the concentration of any particular species in three different ways: 1) through the effect of all NLTE treated species on the chemical equilibrium of the gas by way of the contribution of each species to the e^- reservoir, 2) through changes in the equilibrium structure of the atmosphere as a result of NLTE effects on the total opacity and on the e^- density (see Fig. 5), and 3) through changes in the radiation field in a transition of one species that overlaps an important transition in another species. Examples of the latter include line interlocking and the pumping of transitions, and are especially important for species that have a rich line spectrum such as Fe, Co, and Ni.

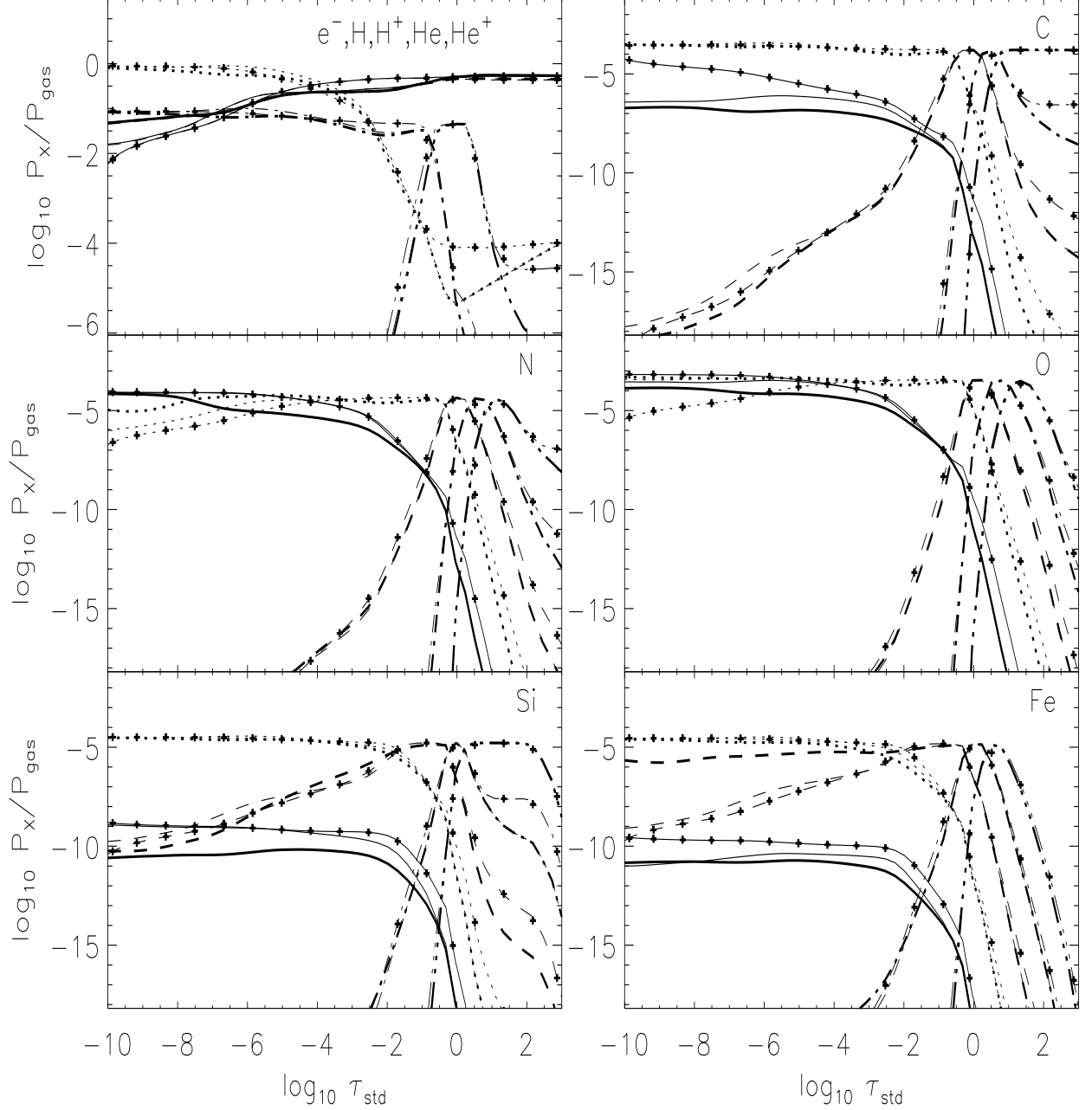


Fig. 1.— Comparison of partial pressure of various species for the *M1* model. Thin lines with \times symbols: LTE, thin lines: HSSBSA NLTE, thick lines: current NLTE. Line style correspond to ionization stages; solid: I, dot: II, dash: III, dot-dash: IV, dot-dot-dot-dash: V, except for upper left panel; solid: e^- , dot: H I, dash: H II, dot-dash: He I, dot-dot-dot-dash: He II.

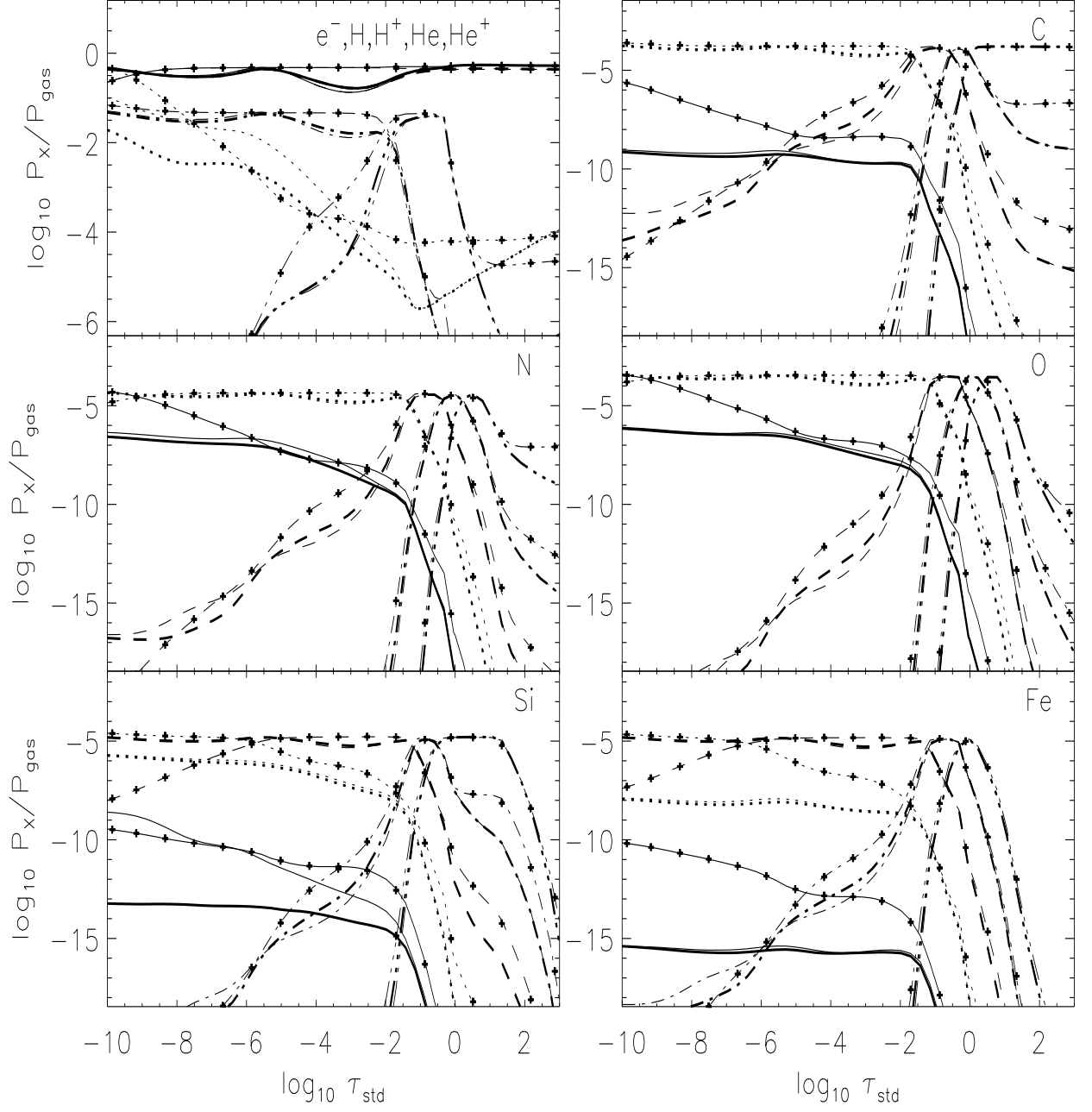


Fig. 2.— Partial pressure of various species for the M2 model. See Fig. 1.

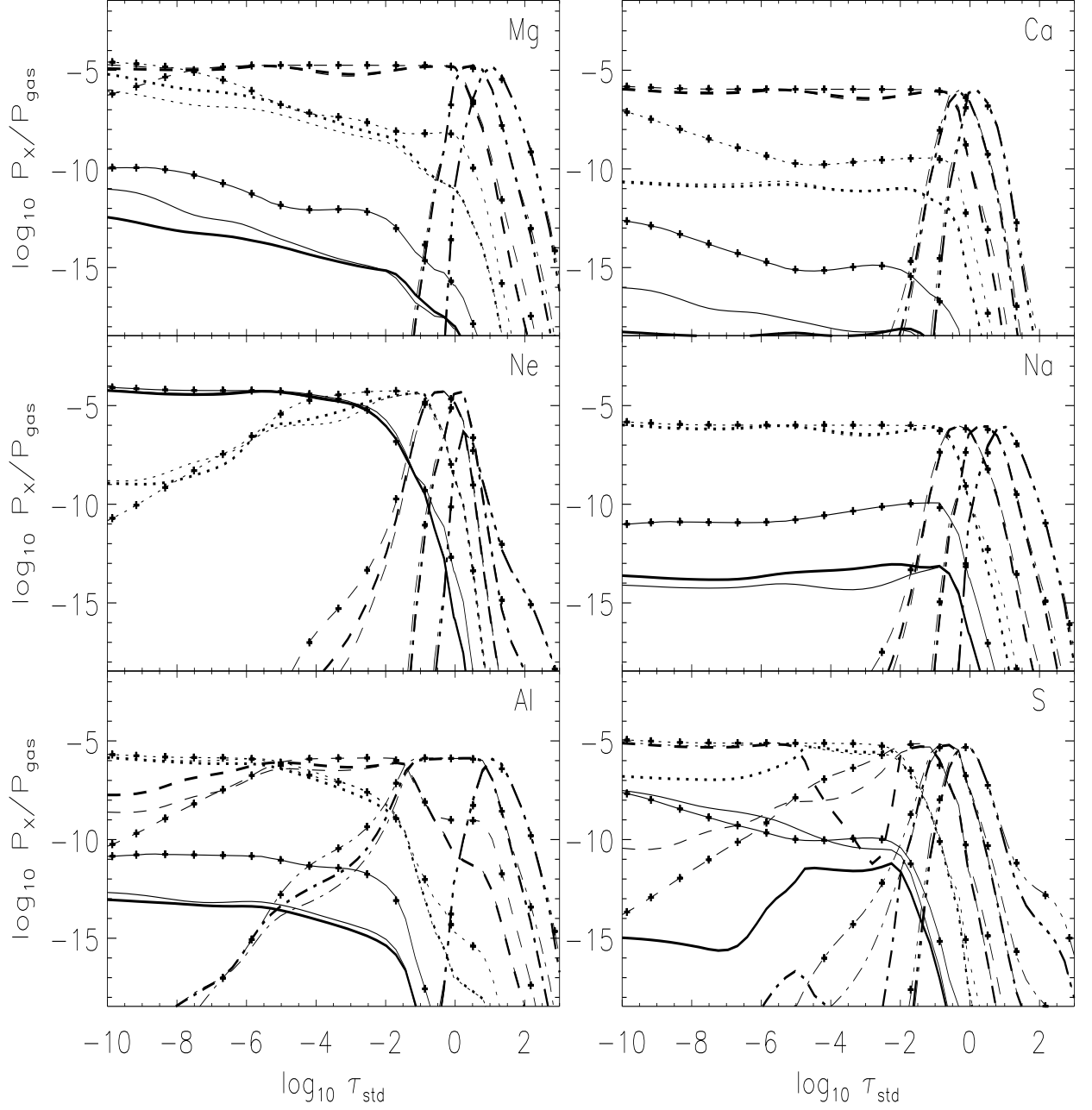


Fig. 3.— Partial pressure of additional species for the M2 model. See Fig. 1.

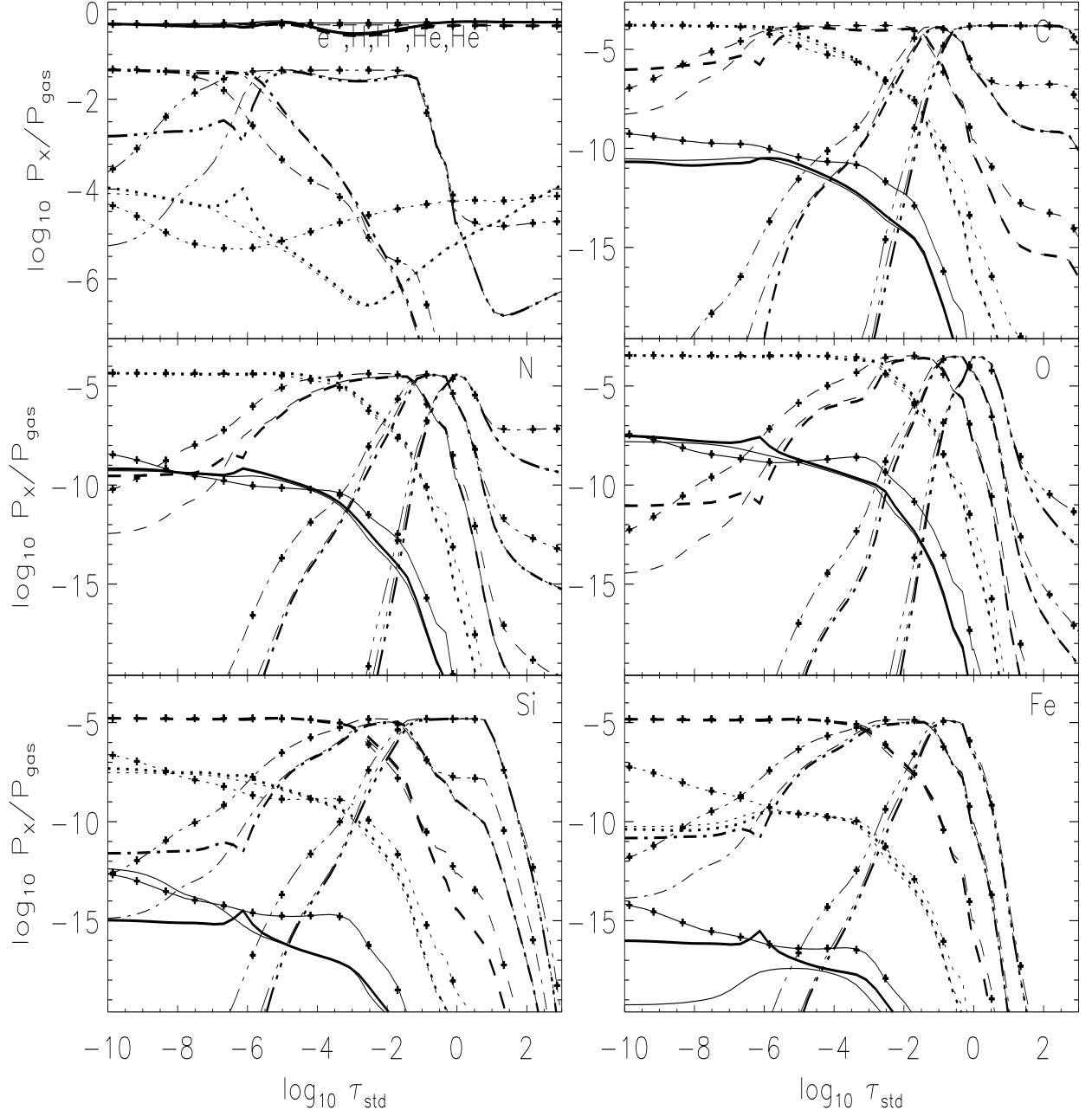


Fig. 4.— Partial pressure of various species for the M3 model. See Fig. 1.

4.1.1. Hydrogen, Helium, and electrons

The upper left panels of Fig. 1 is directly comparable to Fig. 1 of HSSBSA. We confirm the result of HSSBSA that for a model of T_{eff} equal to 15 000 K, NLTE enhances the H I concentration above the LTE values in the outer atmosphere where $\log \tau_{\text{cont},5000} < -6$ and slightly reduces it in the range where $-6 < \log \tau_{\text{cont},5000} < -2$. The largest NLTE effect is the reduction of the H I concentration by as much as 1.5 dex deep in the atmosphere where $-1 < \log \tau_{\text{cont},5000} < 2.5$. We note that the H II concentration is very close to the e^- concentration throughout the atmosphere, which indicates that H ionization is the dominant e^- contributor, even in the $\log \tau_{\text{cont},5000} < -4$ range where H is mostly neutral. As a result, the NLTE reduction of the e^- concentration in the $\log \tau_{\text{cont},5000} < -6$ range and enhancement of it in the $-6 < \log \tau_{\text{cont},5000} < -2$ range is mostly due to NLTE effects on the H ionization equilibrium. We also confirm the HSSBSA result that NLTE slightly reduces the He I concentration around $\log \tau_{\text{cont},5000} = -4$. We also find that NLTE reduces the He II concentration for $\log \tau_{\text{cont},5000} < -1$. However, the He II concentration is declining rapidly in this range as τ decreases due to recombination to He I as $T(\tau)$ decreases. This NLTE effect is not apparent in Fig. 1 of HSSBSA because of the more limited scale of their figure. The inclusion of the new species in NLTE has a negligible effect on the concentration of H I and II, and He I for this model. The new treatment produces a slight effect on the e^- concentration, first reducing it, then enhancing it as $\log \tau_{\text{cont},5000}$ decreases below -5 . We note that changes in the state of the gas at $\log \tau_{\text{cont},5000} < -6$ only affect the profiles of the strongest spectral lines. The He II concentration at $\log \tau_{\text{cont},5000} < -1$ is reduced in the new treatment by approximately as much as the HSSBSA treatment reduced it from the LTE values.

The upper left panels of Fig. 2 shows the same species for the *M2* model. Here, the effects of NLTE, and of the different NLTE treatments are larger. For $\log \tau_{\text{cont},5000} < -4$ where H I becomes relatively abundant, the HSSBSA treatment reduces the H I concentration by as much as two and a half orders of magnitude. However, the current NLTE treatment gives rise to a *smaller* reduction, producing results that are closer to the original LTE concentration. The new treatment also predicts a small enhancement in the concentration around $\log \tau_{\text{cont},5000} = -5$ that is not present in the HSSBSA results. As with the *M1* model, the largest NLTE effect is reduction in H I concentration by as much as ≈ 1.5 dex at greater depth where $-3 < \log \tau_{\text{cont},5000} < 2.5$. Both NLTE treatments give rise to very similar He concentrations and produce a reduction in the He I and II pressures for $\log \tau_{\text{cont},5000} < -1.5$. This reduction is as much as half an order of magnitude in the case of He I. Unlike the *M1* model, the e^- pressure throughout the outer atmosphere is *not* driven by either the H or He ionization equilibria. The two regions of reduction in the e^- concentration at

$-5 < \log \tau_{\text{cont},5000} < -1$ and $-9 < \log \tau_{\text{cont},5000} < -6$ are matched by similar *reductions* in He I concentration and the outermost of these reductions is also matched by a *reduction* in the H I concentration. A NLTE reduction in the population of electrons available for recombinations is driving a reduction in the neutral H and He populations.

Model *M3* is hotter than any of the models discussed in HSSBSA. From the upper left panel of Fig. 4 we see that at $T_{\text{eff}} = 35\,000$ K H is almost completely ionized throughout the entire atmosphere. Neutral H is a very small minority stage and is very sensitive to the treatment of the equilibrium. The NLTE suppression of H I at depth that was noted for the *M1* and *M2* models is more pronounced here: the NLTE H I concentration drops below its LTE value by as much as two orders of magnitude from $-5 < \log \tau_{\text{cont},5000} < 2.5$. The e^- and H^+ populations, which dominate the gas pressure throughout the entire atmosphere, show slight NLTE effects around $-4 < \log \tau_{\text{cont},5000} < -2$ where there is a slight NLTE reduction by as much as ≈ 0.3 dex.

4.1.2. Metals

Carbon, nitrogen, and oxygen (CNO) are important in nova spectra as a measure of convective dredge up of nuclear processed material in the progenitor WD, and as a test of thermonuclear runaway (TNR) models of nova explosions (Starrfield *et al.* 1998, Gehrz *et al.* 1998). The upper right panel of Fig. 2 is directly comparable to Fig. 2 of HSSBSA. We confirm their result that C II is the dominant ionization stage, and that the HSSBSA NLTE treatment reduces the C I and enhances the C III concentration compared to the LTE levels for $\log \tau_{\text{cont},5000} < -2$. The current NLTE treatment produces approximately the same results for C I and C II, but produces a slight NLTE *reduction* in C III throughout most of the range where the HSSBSA treatment produces an enhancement. From examination of Fig. 2 and of Fig. 3 in HSSBSA we see that the same relative behavior for the different NLTE treatments is seen for the lowest three stages of N. From inspection of Fig. 1 and Fig. 4 in HSSBSA we see that NLTE effects for O are much smaller in the cooler *M1* model. We note that the details of the NLTE treatment of CNO are identical in for both HSSBSA and the present calculation; the number of ionization stages and the size of the model atoms are the same in both treatments. The large differences seen in the concentration of some CNO stages in the *M2* model are entirely due to the *indirect* effects of other species treated in NLTE by way of either the chemical equilibrium or the atmospheric structure.

The rich blanketing of line opacity contributed by Fe plays a crucial role in the time development of the *UV* and optical light curves and spectra during the outburst (Hauschildt *et al.* 1994, Shore *et al.* 1994). From inspection of the lower right panel in Figs. 1 and 2 we see that Fe II is the dominant ionization stage throughout most of the outer atmosphere in the *M1* model, whereas Fe III plays the same role in the *M2* and *M3* models. For the *M1* model, the HSSBSA NLTE treatment leads to a significant enhancement of the Fe I concentration above LTE values for $\log \tau_{\text{cont},5000} < -2$, whereas the current treatment leads to a *reduction* in this range and to a concentration that is much closer to LTE. Both treatments lead to significant enhancements in the Fe III concentration throughout the outer atmosphere. For the *M2* and *M3* models, NLTE effects in both treatments lead to a large reduction in both the Fe I and Fe II concentrations for $\log \tau_{\text{cont},5000} < -2$. However, the current NLTE treatment gives rise to an Fe I reduction that is approximately twice as large as the that of the HSSBSA treatment. We note that Fe II in particular has a very rich *UV* line spectrum that determines the *UV* flux distribution and affects the atmospheric structure during the optically thick wind phase of the outburst (Hauschildt *et al.* 1994, Shore *et al.* 1994). Therefore, the reduction in Fe II concentration by two orders of magnitude that is produced by both NLTE treatments in the *M2* and *M3* models will have a significant effect on the model structure. This is also discussed by HSSBSA. As was the case with CNO, differences between the two NLTE treatments may be due to the indirect effects of other NLTE species. In addition, the difference in the Fe I- III results may also be due to the presence of a detailed Fe IV model atom in the NLTE calculation.

In Figs. 2 and 3 we show concentrations for a variety of other species treated in NLTE for the *M2* model. NLTE results for S and Si were shown in HSSBSA, but they only treated the second and third ionization stages in NLTE, whereas we treat the lowest six stages. These two elements provide an object lesson in the importance of adjacent ionization stages to the accurate treatment of a particular stage in NLTE. In their Fig. 5 HSSBSA show an increase in the concentration of S I with respect to LTE by as much as three orders of magnitude for $\log \tau < -3$ when S II and III are treated in NLTE. Our results for the *M2* model, shown in the bottom right panel of Fig. 3, are not exactly comparable because *M2* has a T_{eff} that is 5000 K cooler than the model for which HSSBSA show results. However, our treatment, in which S I is included in NLTE, produces a seven orders of magnitude *decrease* in the S I concentration in the outer atmosphere. Moreover, whereas, HSSBSA found an increase by ≈ 1 order of magnitude in the S III concentration in the same τ range, our calculations, in which S IV is included in NLTE, show an increase by as much as nine orders of magnitude in the outer atmosphere. Comparison of Fig. 6 in HSSBSA to the bottom left panel of Fig. 2 shows similar effects for Si. For example, whereas the

HSSBSA treatment, in which Si I is in LTE, yields an increase with respect to LTE in the Si I concentration in the outer atmosphere of a 25 000 K model, we find that the *M2* model with Si I to IV in NLTE shows a *decrease* by as much as five orders of magnitude. We note that S I and Si I are both minority stages in these models. In general, the population of a minority stage is very sensitive to the photoionization rate and to the population of the reservoir stage.

Aluminum and the higher stages of Na are treated in NLTE for the first time. Magnesium and Ca both have *UV* resonance lines from the second ionization stage that are important spectral features. HSSBSA treated only the second stage in NLTE, whereas we treat the lowest six. Inspection of these figures shows that for all of these species, NLTE effects, and the particular treatment of NLTE, are significant for one or more stages.

4.2. Atmospheric structure

Fig. 5 shows the atmospheric structure of our models. From the left panels we see that the HSSBSA NLTE treatment gives rise to surface heating with respect to LTE for $\log \tau_{\text{cont},5000} < -6$ in the *M2* model. By contrast, the current NLTE treatment gives rise to a T_{kin} structure that is cooler in the upper atmosphere. The HSSBSA treatment yields a surface cooling with respect to LTE in the *M3* model whereas the more complete NLTE treatment produces higher T_{kin} values in the upper atmosphere. For both models, the more complete NLTE treatment gives rise to a T_{kin} structure that is *closer* to the LTE structure than that of the less complete NLTE treatment. We note that the presence or absence of this NLTE surface heating or cooling in the models will affect the cores of strong lines that form near the top of the atmosphere. NLTE effects on the T_{kin} structure are negligible in the *M1* model. From the right panels of Fig. 5 we see that NLTE effects cause a slight reduction in P_{gas} around $\log \tau_{\text{cont},5000} = -2$ in the *M1* model and a general reduction throughout the atmosphere in the *M2* model for $\log \tau_{\text{cont},5000} < -2$. Both NLTE treatments give approximately the same result. For the *M3* model, both NLTE treatments give pressure structures that are close to the LTE structure except for a slight reduction around $-4 < \log \tau_{\text{cont},5000} < -2$. By comparing the P_{gas} and P_e structure, we note that the NLTE deviations in P_{gas} in all models mirror those in P_e . The NLTE behavior of P_e was discussed above in connection with NLTE H and He.

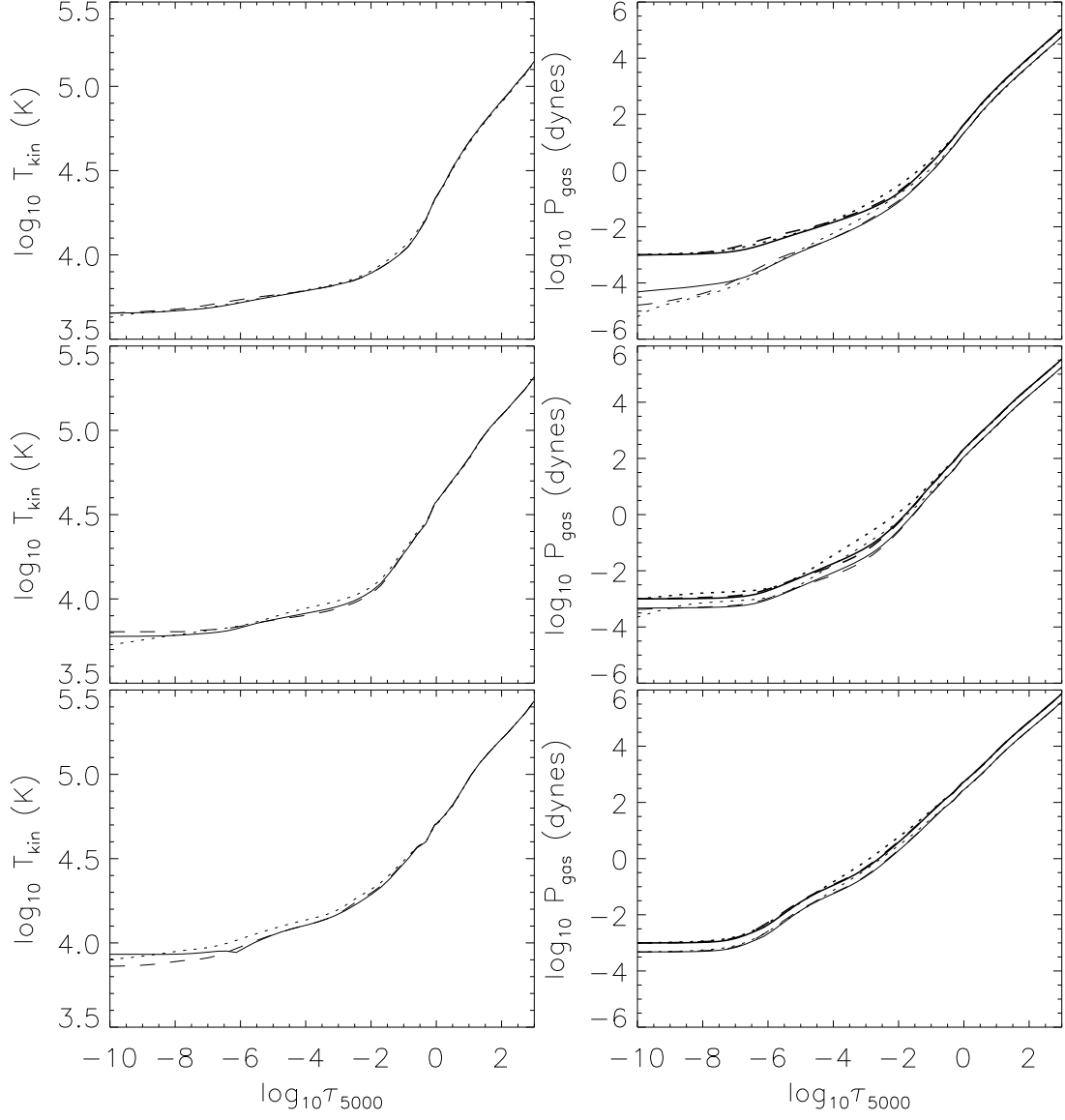


Fig. 5.— Atmospheric structure of models. Left panels: kinetic temperature, right panels: gas and e^- pressure. Upper panels: $M1$ model, middle panels: $M2$ model, lower panels: $M3$ model. Solid line: current NLTE, dashed line: HSSBSA NLTE, dotted line: LTE. In the right panels: thin lines: e^- pressure, thick lines: total gas pressure.

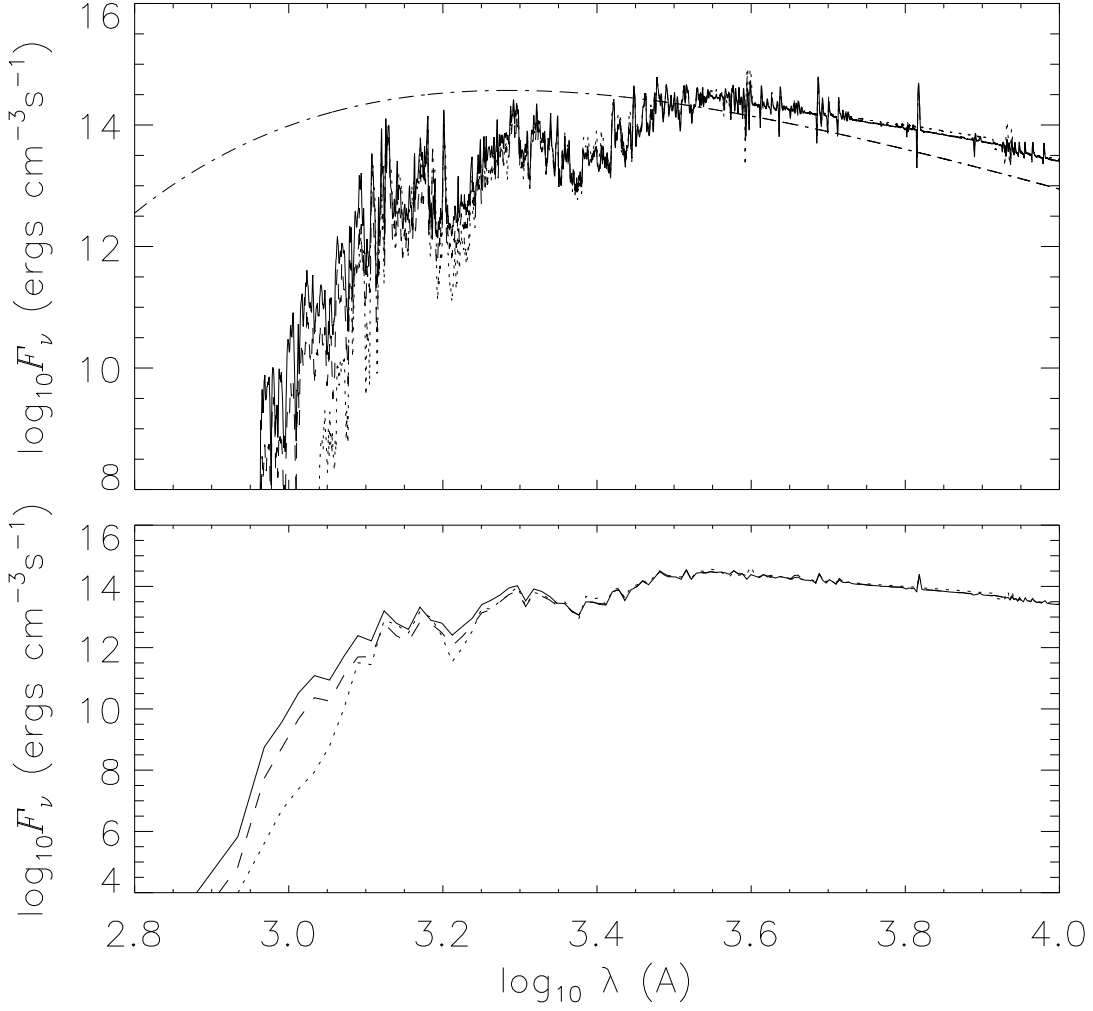


Fig. 6.— Flux distribution, F_λ , of $M1$ model. Upper panels: flux distribution computed with $\Delta\lambda = 1.0\text{\AA}$ for $\lambda < 900\text{\AA}$ and with $\Delta\lambda = 0.5\text{\AA}$ for $\lambda > 900\text{\AA}$. Lower panels: flux distribution smoothed with a boxcar of $\Delta\lambda = 100\text{\AA}$ in the far UV and $\Delta\lambda = 50\text{\AA}$ in the near UV , optical, and IR . Solid line: current NLTE, dashed line: HSSBSA NLTE, dotted line: LTE, dot-dashed line: Planck function (B_λ).

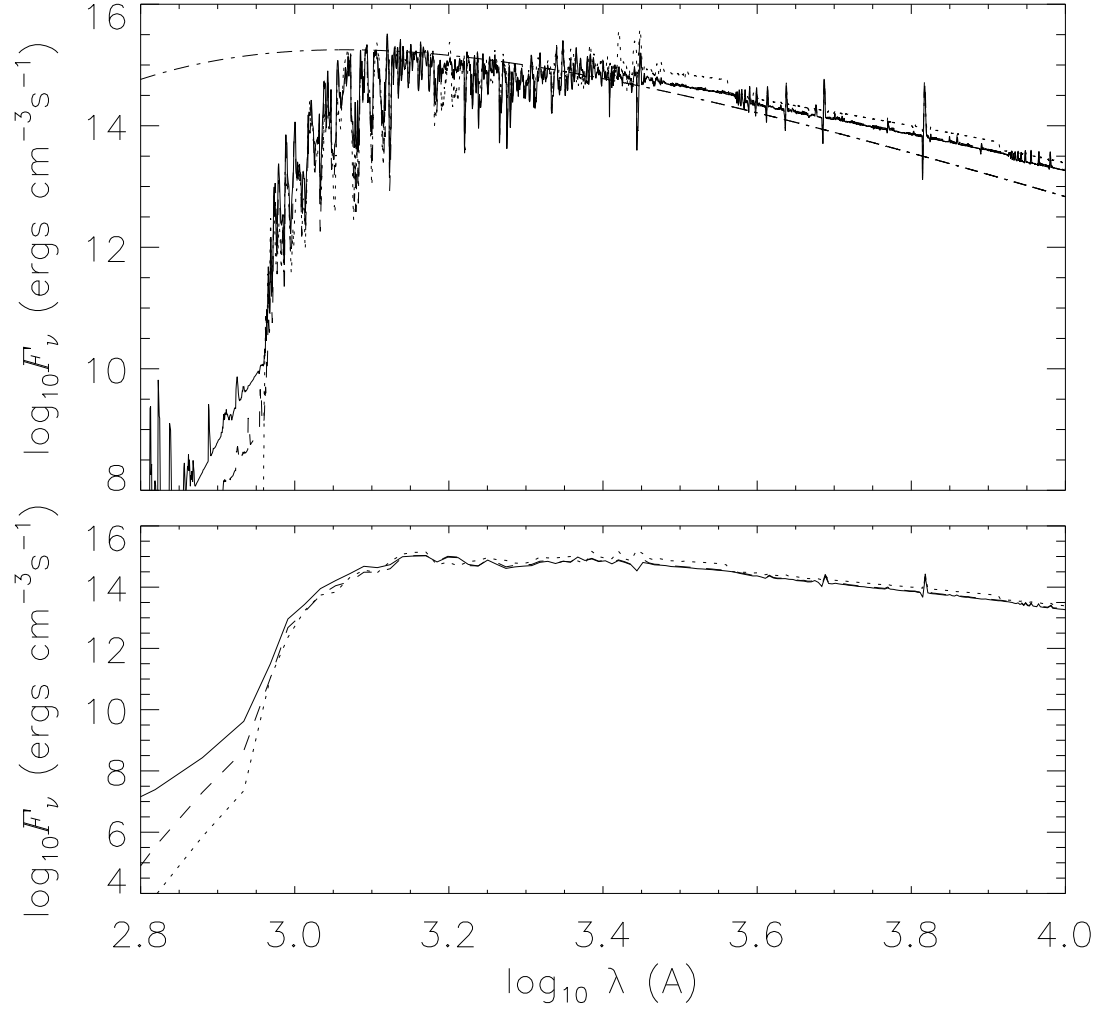


Fig. 7.— Flux distribution, F_{λ} , of $M2$ model. See Fig. 6.

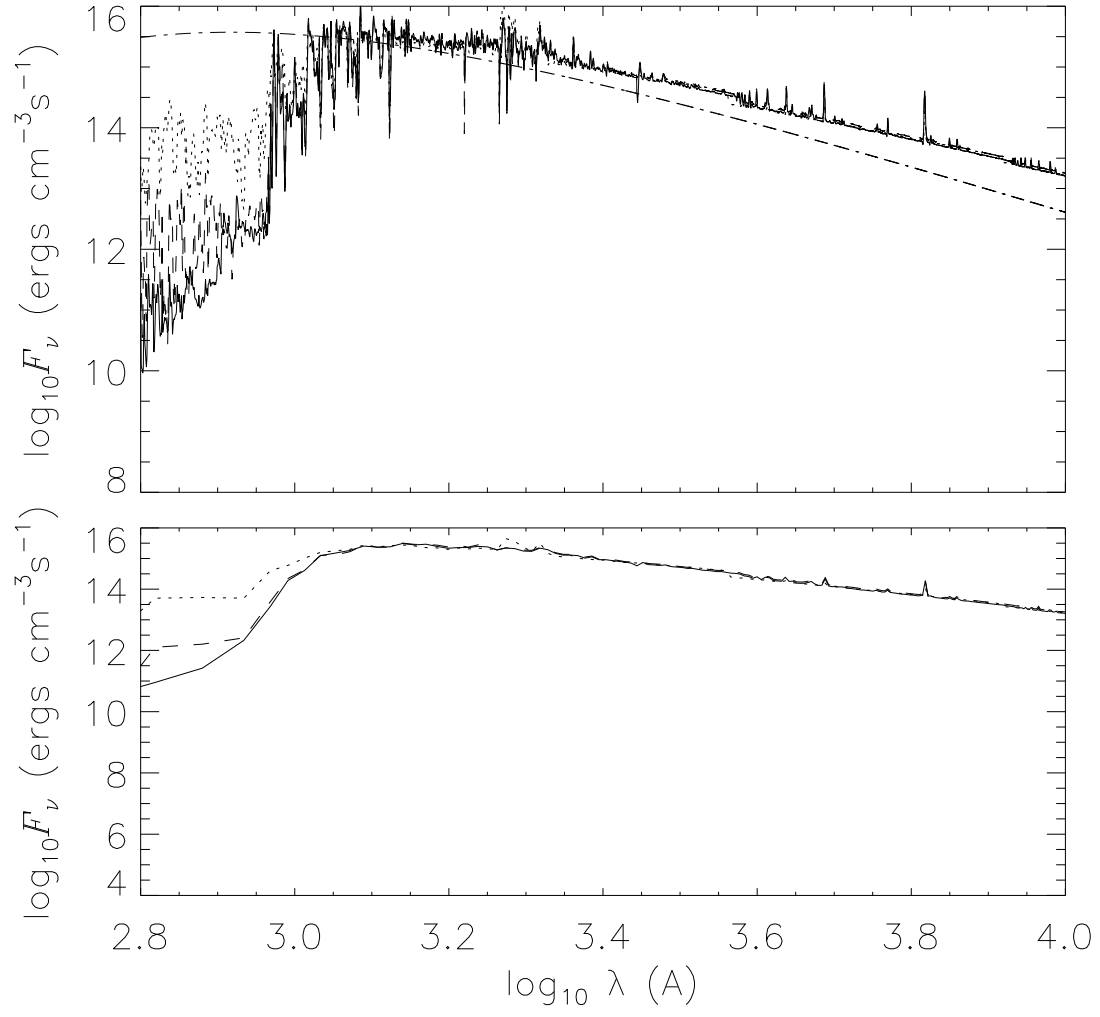


Fig. 8.— Flux distribution, F_λ , of *M3* model. See Fig. 6.

4.3. Flux distribution

Figs. 6 to 8 show the distribution of the emergent flux, $F_\lambda(\tau = 0)$ produced by the models in the observer’s (Eulerian) frame. In the upper panel we show F_λ at the computed resolution of $\Delta\lambda = 1.0\text{\AA}$ for $\lambda < 900\text{\AA}$, and $\Delta\lambda = 0.5\text{\AA}$ for $\lambda > 900\text{\AA}$. The effect of massive line blanketing on the spectrum can be seen for $\log \lambda < 3.5$. In the lower panel we show the same F_λ distributions after smoothing with a boxcar function of width $\Delta\lambda = 100\text{\AA}$ in the far *UV* and $\Delta\lambda = 50\text{\AA}$ in the near *UV*, optical and near infrared (*IR*). The smoothing approximately reproduces the resolution of intermediate band photometry and wide band spectrophotometry and allows differences in the overall F_λ level to be more easily discerned.

From the lower panels we see that NLTE effects lead to large enhancements in F_λ for $\log \lambda < 3.1$ in the *M1* model and for $\log \lambda < 2.95$ in the *M2* model. By contrast, NLTE effects lead to a *reduction* in the UV flux in the *M3* model for $\log \lambda < 2.95$. For all three models, the current NLTE treatment increases the size of the NLTE deviation in F_λ significantly. The opacity sources that have the largest effect on the emergent flux below the Lyman edge ($\log \lambda < 2.95$) are H I *b* – *f* absorption and line absorption. We see from Figs. 1 through 4 that the H I concentration is always significantly reduced by the effect of NLTE at depths where $\tau_{\text{cont},5000} \leq 1$, and is often enhanced higher up in the atmosphere. Furthermore, the current NLTE treatment serves variously to enhance or diminish the size of the NLTE deviation in H I concentration. We may expect that, all else being equal, models in which the emergent flux in the Lyman continuum arises from deeper in the atmosphere will be brighter in the UV in the case of NLTE because the reduction in H I will allow flux to escape from deeper, hotter layers. By contrast, models in which this flux arises from higher up in the atmosphere will be dimmer in the case of NLTE. The extent of the NLTE effect on the emergent flux for particular NLTE treatments will be modified by how that treatment effects the H I concentration.

The situation is complicated by the competing effect of line opacity in determining the emergent UV flux. The net effect of NLTE departures on all the metals that contribute significant line opacity may serve either to brighten or dim the flux. From an examination of the concentrations of the dominant Fe ionization stages in Figs. 1 through 4, we see that in the case of *M1* the amount of Fe line blanketing is enhanced by the current NLTE treatment compared to the other two treatments, and in *M2* and *M3* Fe line blanketing is reduced by both NLTE treatments. It is not clear how this can be reconciled with the effects of NLTE on the flux seen in Figs. 6 through 8, and we conclude that the competing influence of NLTE on all the various absorbers that contribute significant opacity is too

complex for a simple correlation between the emergent flux and the concentration of any one absorber to be apparent. Finally, we note that generally the flux on the Wien side of the Planck distribution is a sensitive indicator of T_{eff} . Therefore, the significant NLTE effects on the UV flux seen here must be included accurately in models.

4.4. Completeness

Fig. 9 shows the overall F_λ distribution for the $M2$ model with complete line blanketing due to all species that contribute significant line opacity (whether they are treated in LTE or NLTE), and with line blanketing due *only* to those species treated in NLTE, as indicated in Table 3. A comparison of the two distributions allows an assessment of the completeness of the line opacity that is now treated in NLTE. This is important for assessing the accuracy of the emergent flux spectrum, and also of the equilibrium atmospheric structure because line opacity is an important term in the radiative equilibrium of the atmosphere.

The most obvious difference between the two F_λ distributions is that the Lyman photo-ionization edge at $\log \lambda = 2.96$ is “softened” by line blanketing to a greater extent when LTE lines are present. The missing NLTE UV line opacity will mostly be accounted for once Fe group species that have a rich line spectrum, such as Cr III and Ni II and III and Co II have been added in NLTE. From Table 1 it can be seen that we already have the facility to compute Ni in NLTE up to stage VI and Co up to stage III, but, as noted in Section 3 and in Table 3, these stages have not been included in these calculations for the sake of computational expediency. Also, there is a noticeable underblanketing in the $3.1 < \log \lambda < 3.5$ range in the treatment with NLTE lines only compared to the fully blanketed treatment. Nevertheless, from the qualitative similarity of the two F_λ distributions we can also see that the lines treated in NLTE account for the vast majority of the total line opacity.

4.5. UV and optical spectra

Figs. 10 to 12 show the moderate resolution spectrum in three sample regions from the mid-UV to the near-IR. Like HSSBSA we find that the quasi-LTE spectrum with a single scattering albedo incorporated into the line source function gives rise to lines that are approximately equal in strength to NLTE lines. The quasi-LTE approach gives rise to inaccurate line strengths for many particular lines, but does not systematically over-predict or under-predict line absorption. Inspection of Figs. 10 and 11 shows that

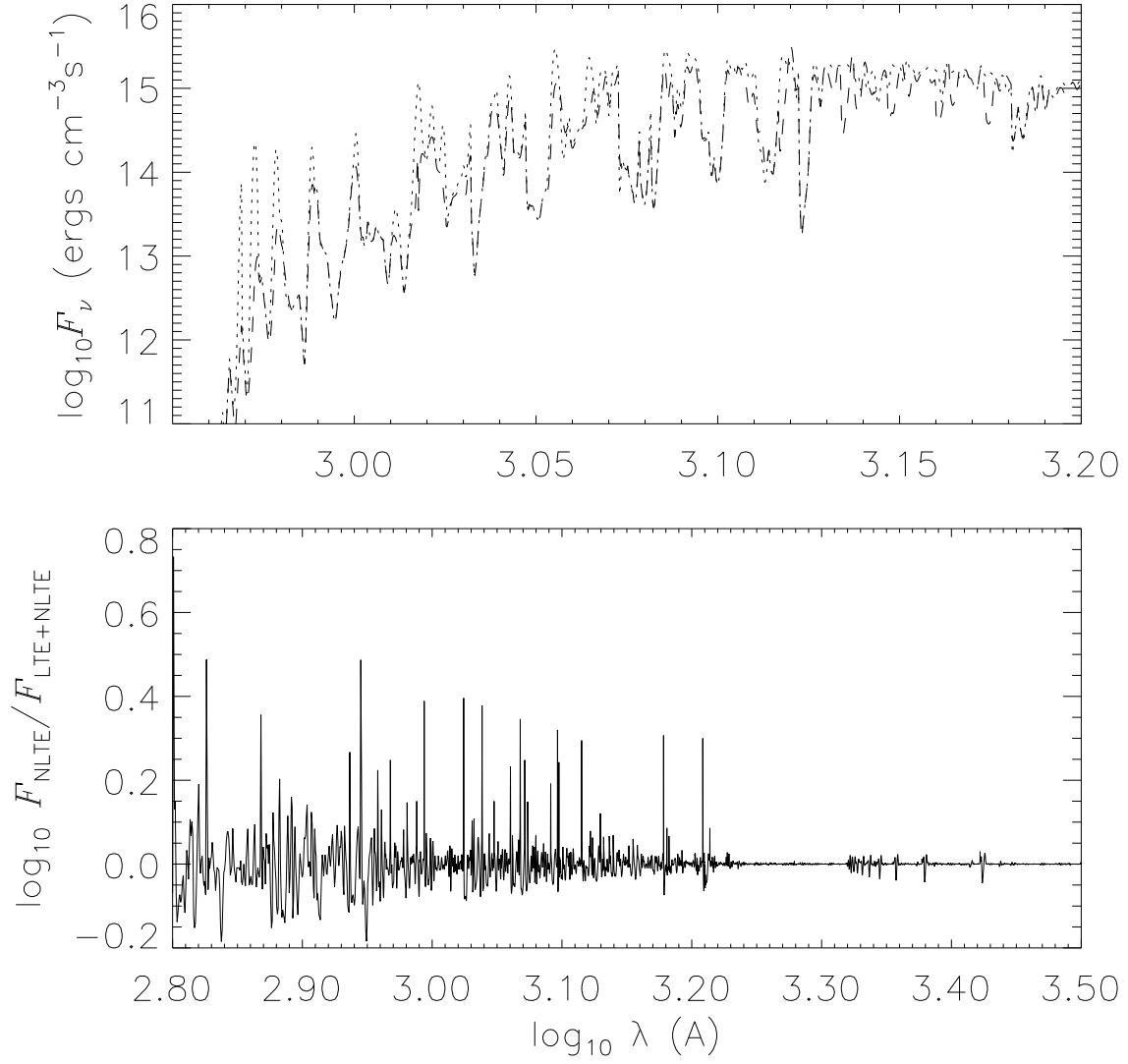


Fig. 9.— Flux distribution, F_λ , of $M2$ model with different treatments of line blanketing. Upper panel: F_λ with NLTE lines only: dotted line; F_λ with LTE and NLTE lines (complete blanketing): dashed line. Lower panel: Ratio of F_λ computed with NLTE lines only to F_λ computed with all lines.

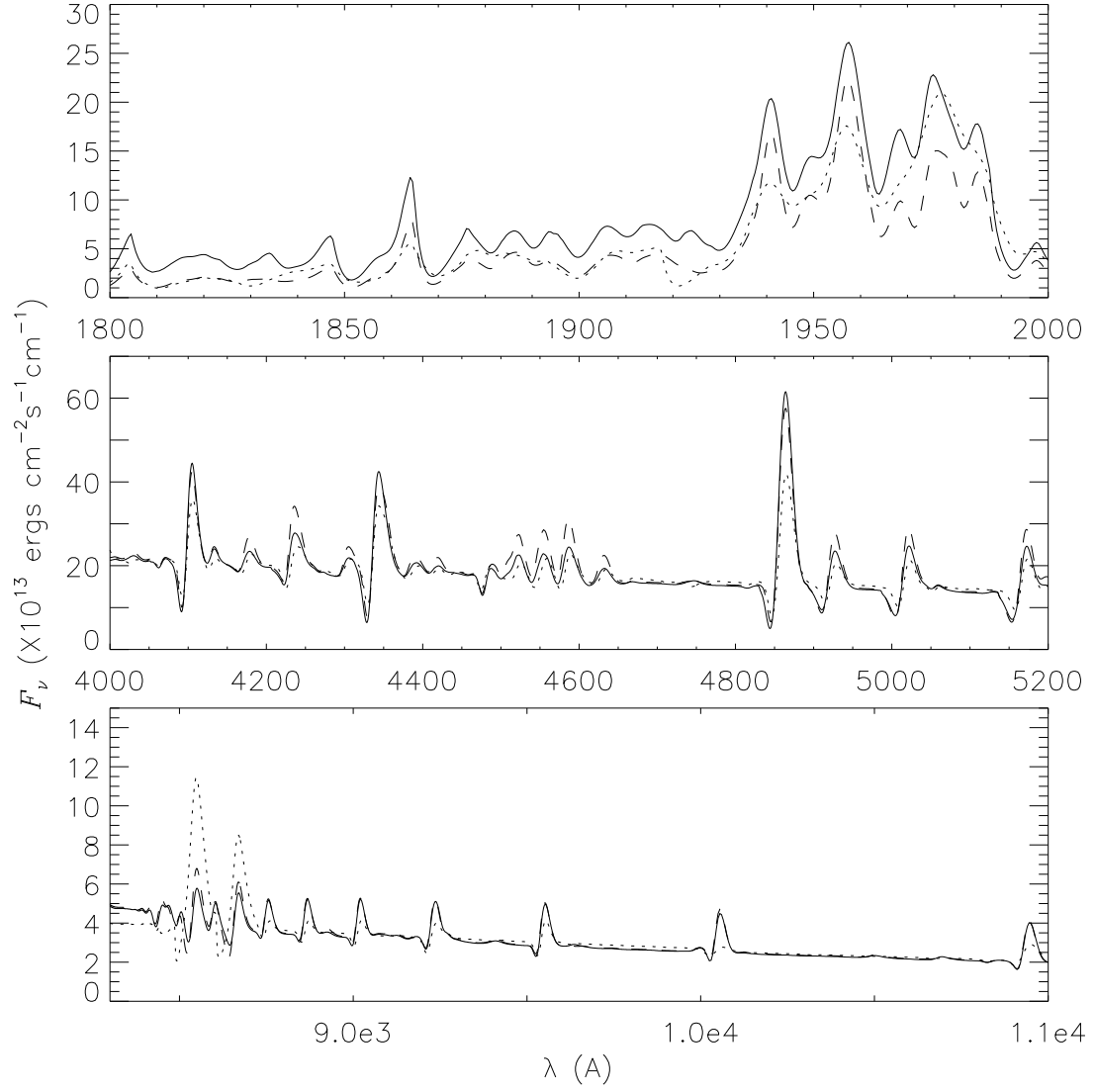


Fig. 10.— Flux spectrum of *M1* model in three sample regions from the mid-*UV* to near *IR*. Solid line: current NLTE, dashed line: HSSBSA NLTE, dotted line: LTE,

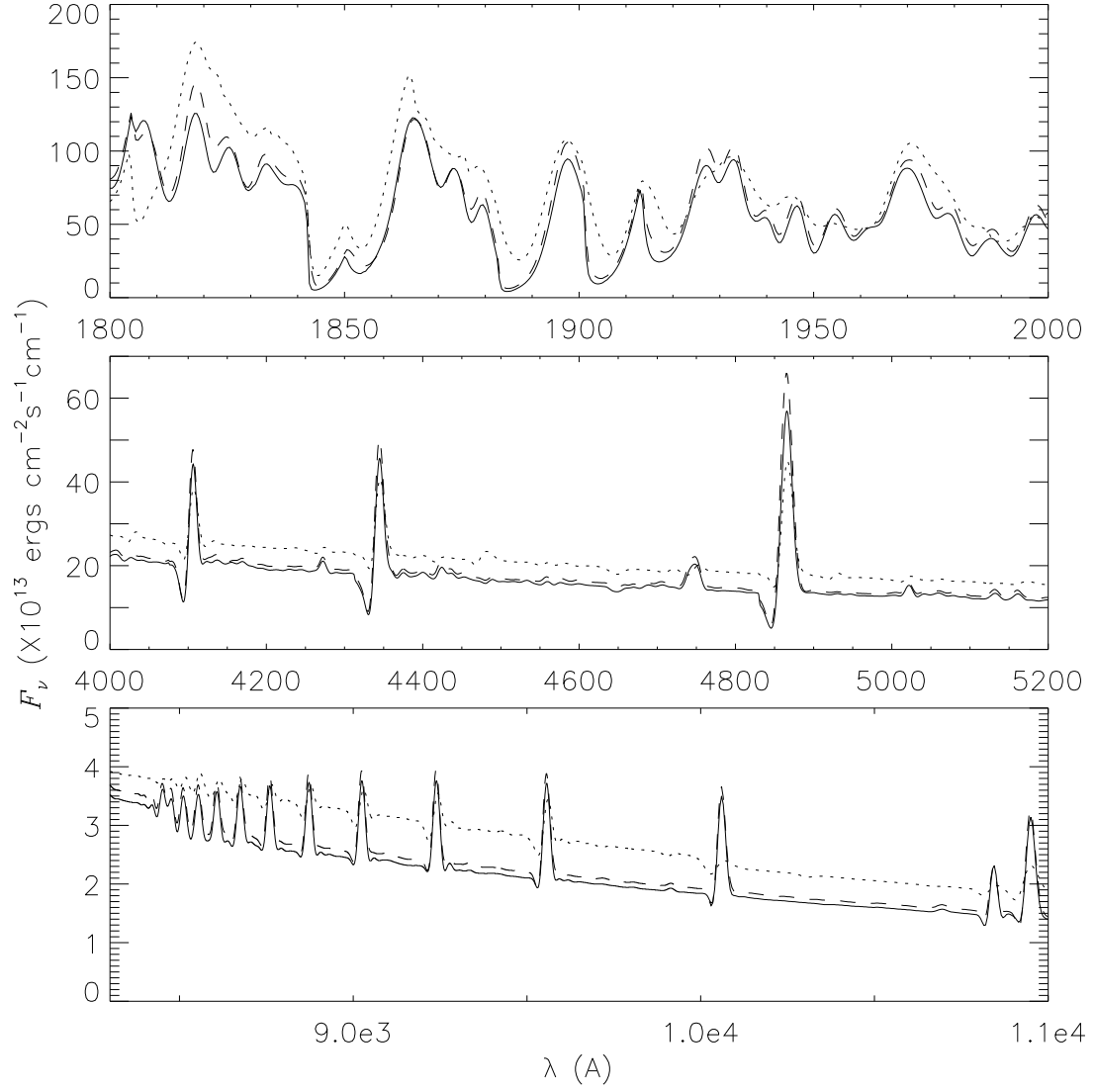


Fig. 11.— Flux spectrum of *M2* model in three sample regions from mid-*UV* to near *IR*.
See Fig. 10

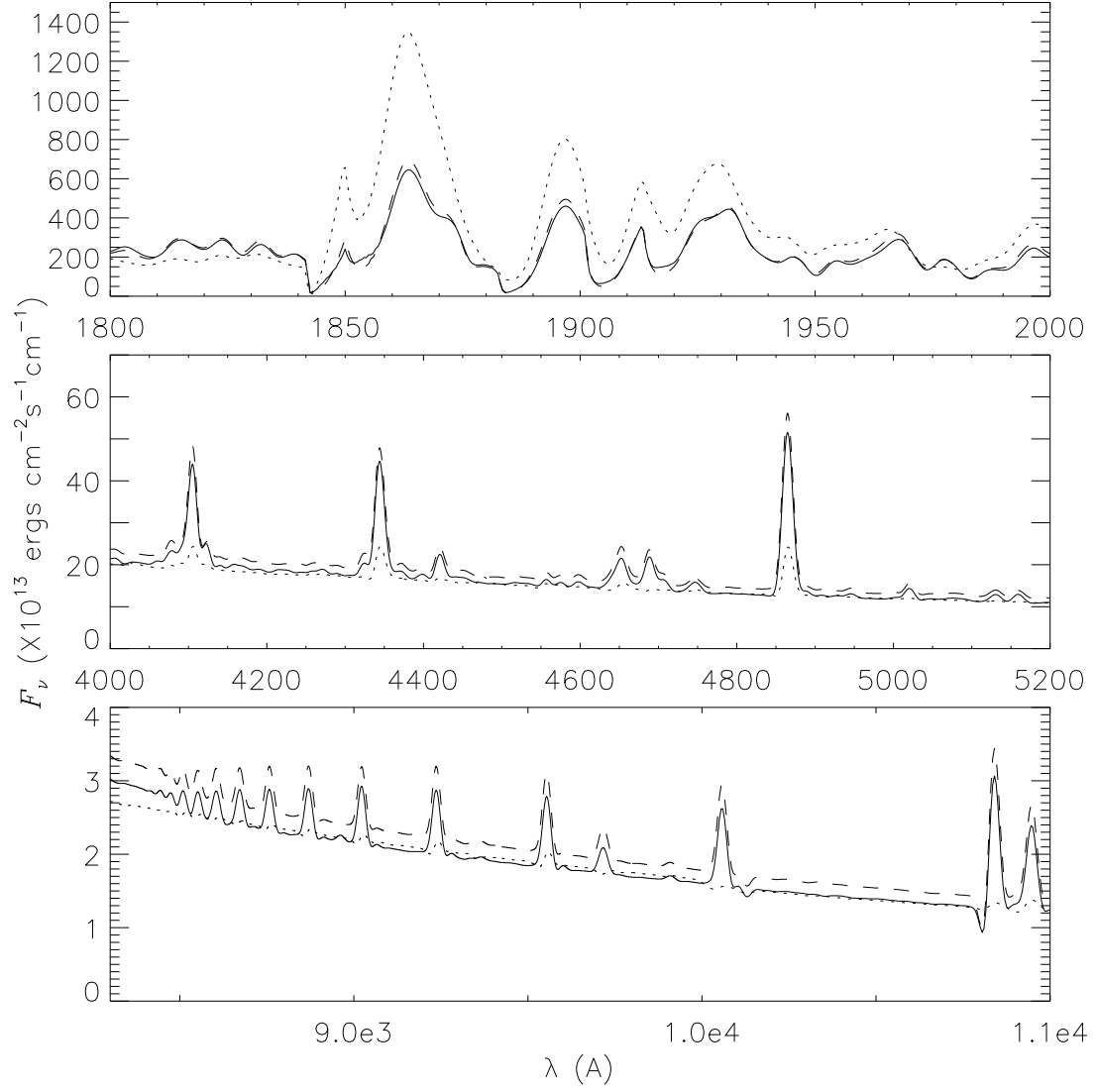


Fig. 12.— Flux spectrum of *M3* model in three sample regions from mid-*UV* to near *IR*.
See Fig. 10

the HSSBA and the current NLTE treatment give rise to different line profiles for many lines, but the differences are not systematic. Differences between the two NLTE treatments are particularly apparent in the *UV* region of the *M2* model as shown in the top panel of Fig. 11. Note that differences in the profiles of individual lines that arise from the NLTE treatment may in general be due to a combination of effects: 1) changes in the line source function, $S_\nu(\tau)$, as a result of changes in the populations, n_l and n_u , of the levels connected by the transition and by the inclusion of a properly calculated scattering contribution in $S_\nu(\tau)$, 2) changes in the background continuous and line opacity due to NLTE effects in other species, and 3) changes in the atmospheric structure such as those discussed in Section 4.2. In general, NLTE effects should be included in as complete a way as possible to accurately calculate any particular line profile.

5. Conclusions

Generally, we find that the current, more complete NLTE calculation gives rise to *qualitatively* the same results as the previous extensive NLTE investigation of nova models, that of HSSBSA. NLTE may greatly affect: 1) the chemical concentration of species that are important to the total opacity of the model, such as H I and Fe, or are astrophysically interesting, such as CNO, Mg, Al, and Ca, 2) the overall flux distribution, particularly in the *UV* ($\lambda < 1000\text{\AA}$), which is a sensitive T_{eff} indicator, and where NLTE effects increase the flux by several orders of magnitude, 3) the strength of individual lines throughout the observable *UV* to *IR* region where NLTE causes particular lines to be either weaker or stronger than those of a quasi-LTE calculation that crudely incorporates NLTE effects with a single scattering albedo, and 4) to a lesser extent, the atmospheric structure, particularly the P_{gas} structure in models of $T_{\text{eff}} \approx 25\,000$ K. However, the current NLTE treatment gives rise to specific deviations from LTE values for many of these quantities that differ significantly from those of the HSSBSA treatment. In particular, we note that for the hotter *M2* model ($T_{\text{eff}} = 25\,000$ K), in which NLTE effects are generally larger than for the cooler *M1* model ($T_{\text{eff}} = 15\,000$ K), the more complete NLTE treatment gives rise to an H I concentration, T_{kin} and P_{gas} structure, and *UV* flux level that are all significantly *closer* to the LTE values than those of the less complete HSSBSA NLTE treatment. This result, which may seem counterintuitive at first, results from the increased number of channels through which the gas can thermalize when more species are included in the overall NLTE solution. Note that increasing the number of NLTE species does not necessarily drive the solution for any model atmosphere closer to LTE. Rather, for the *M2* model in particular, the increase in the number of thermalization channels happens to have a dominant effect on the solution when the number of NLTE species is increased from the HSSBSA set to the

current set.

In general, NLTE should be incorporated in as complete a way as possible for accurate structure and synthetic spectrum calculations for nova models in the 15 000 to 35 000 K T_{eff} range. In regard to the first point above, we draw special attention to the *indirect* effects that treating any one species in NLTE may have on any other species. The atmospheric structure and the e^- concentration both act as means of coupling all the species, including those that are treated in LTE. Generally, all species that contribute significantly to the e^- reservoir by way of partial ionization, or whose line or continuous opacity is large enough to significantly effect the equilibrium structure of the atmosphere, must be treated in NLTE to insure an accurate result for any particular species. This has a bearing on, for example, attempts to infer model parameters and abundances from fitting the *UV* and optical light curves of novae during the optically thick wind phase of their outburst.

This work was supported in part by NASA ATP grant NAG 5-3018 and LTSA grant NAG 5-3619 and NSF grant AST-9720804 to the University of Georgia, and by NSF grant AST-9417242, NASA grant NAG5-3505 and an IBM SUR grant to the University of Oklahoma. Some of the calculations presented in this paper were performed on the IBM SP2 and SGI Origin 2000 of the UGA UCNS, at the San Diego Supercomputer Center (SDSC) and at the National Center for Supercomputing Applications (NCSA), with support from the National Science Foundation, and at the NERSC with support from the DoE. We thank all these institutions for a generous allocation of computer time.

REFERENCES

- Allen, C. W. 1973, *Astrophysical Quantities*, Athlone Press, London, third edition
- Baron, E., Hauschildt, P.H. 1998, *ApJ*, 495, 370
- Bautista, M. A., Romano, P., & Pradhan, A. K. 1998, *ApJS*, 118, 259
- Drawin, H. W. 1961, *Zs. f. Phys.* 164, 513
- Gehrz, R. D., Truran, J. W., Williams, R. E., & Starrfield, S. 1998, *PASP*, 110, 3
- Hauschildt, P. H. 1993, *JQSRT*, 50, 301
- Hauschildt, P. H. 1992, *JQSRT*, 47, 433

- Hauschildt, P. H. & Baron, E. 1995, JQSRT, 54, 987
- Hauschildt, P. H., Baron, E., & Allard, F. 1997a, ApJ, 483, 390
- Hauschildt, P.H., Shore, S. N., Schwarz, G. J., Baron, E., Starrfield, S., & Allard, F. 1997b, ApJ, 490, 803 (HSSBSA)
- Hauschildt, P. H., Starrfield, S., & Austin, S. 1994, ApJ422, 831
- Hauschildt, P. H., Starrfield, S., Shore, S. N., Allard, F., & Baron, E. 1995, ApJ, 447, 829
- Hubeny, I., Hummer, D. G., & Lanz, T. 1994, A&A, 282, 151
- Kurucz, R. L. & Bell, B. 1995, Atomic line list, Kurucz CDROM No. 23
- Kurucz, R. L. 1994, Atomic data for Fe and Ni, Kurucz CDROM No. 22
- Mathisen, R. 1984, Photo Cross Sections for Stellar Atmosphere Calculations- Compilation of References and Data, Inst. of Theoret. Astrophys., Univ. of Oslo, Publ. Ser. No. 1
- Reilman, R. F. & Manson, S. T. 1979, ApJS, 40, 815
- Seaton, M. J., Yu Yan, Mihalas, D., & Pradhan, A. K. 1994, MNRAS, 266, 805
- Shore, S. N., Sonneborn, G., Starrfield, S., Gonzalez-Riestra, R., & Polidan, R. S. 1994, ApJ421, 344
- Starrfield, S., Truran, J. W., Wiescher, M. C., & Sparks, W. M. 1998, MNRAS, 296, 502
- Van Regemorter, H. 1962, ApJ, 136, 906